

## In situ polarized $^3\text{He}$ system for the Magnetism Reflectometer at the Spallation Neutron Source

X. Tong, C. Y. Jiang, V. Lauter, H. Ambaye, D. Brown et al.

Citation: *Rev. Sci. Instrum.* **83**, 075101 (2012); doi: 10.1063/1.4731261

View online: <http://dx.doi.org/10.1063/1.4731261>

View Table of Contents: <http://rsi.aip.org/resource/1/RSINAK/v83/i7>

Published by the [American Institute of Physics](#).

---

### Related Articles

First results of the SOL reflectometer on Alcator C-Mod

*Rev. Sci. Instrum.* **83**, 10E309 (2012)

Metamaterial near-field sensor for deep-subwavelength thickness measurements and sensitive refractometry in the terahertz frequency range

*Appl. Phys. Lett.* **100**, 221101 (2012)

High-pressure cell for neutron reflectometry of supercritical and subcritical fluids at solid interfaces

*Rev. Sci. Instrum.* **83**, 045108 (2012)

ARGon3: "3D appearance robot-based gonireflectometer" at PTB

*Rev. Sci. Instrum.* **83**, 045102 (2012)

Refractive index sensor based on hybrid coupler with short-range surface plasmon polariton and dielectric waveguide

*Appl. Phys. Lett.* **100**, 111108 (2012)

---

### Additional information on *Rev. Sci. Instrum.*

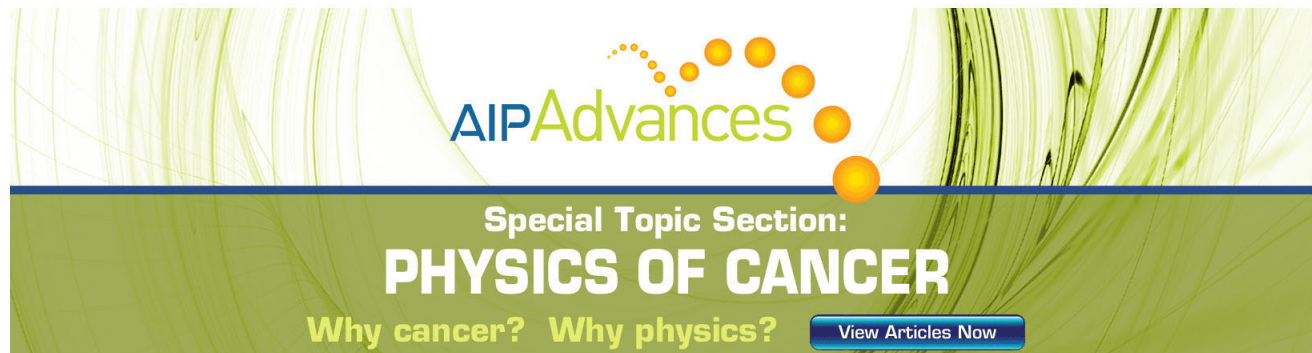
Journal Homepage: <http://rsi.aip.org>

Journal Information: [http://rsi.aip.org/about/about\\_the\\_journal](http://rsi.aip.org/about/about_the_journal)

Top downloads: [http://rsi.aip.org/features/most\\_downloaded](http://rsi.aip.org/features/most_downloaded)

Information for Authors: <http://rsi.aip.org/authors>

## ADVERTISEMENT



**AIPAdvances**

Special Topic Section:  
**PHYSICS OF CANCER**

Why cancer? Why physics?

[View Articles Now](#)

# ***In situ* polarized $^3\text{He}$ system for the Magnetism Reflectometer at the Spallation Neutron Source**

X. Tong,<sup>1,a)</sup> C. Y. Jiang,<sup>1</sup> V. Lauter,<sup>2</sup> H. Ambaye,<sup>3</sup> D. Brown,<sup>1</sup> L. Crow,<sup>1</sup> T. R. Gentile,<sup>4</sup>  
R. Goyette,<sup>3</sup> W. T. Lee,<sup>5</sup> A. Parizzi,<sup>3</sup> and J. L. Robertson<sup>1</sup>

<sup>1</sup>*Instrument and Source Design Division, Oak Ridge National Laboratory, Oak Ridge, Tennessee 37831-6393, USA*

<sup>2</sup>*Quantum Condensed Matter Division, Oak Ridge National Laboratory, Oak Ridge, Tennessee 37831-6393, USA*

<sup>3</sup>*Research Accelerator Division, Oak Ridge National Laboratory, Oak Ridge, Tennessee 37831-6393, USA*

<sup>4</sup>*National Institute of Standards and Technology, Gaithersburg, Maryland 20899-8461, USA*

<sup>5</sup>*Australian Nuclear Science and Technology Organisation, New Illawarra Road, Lucas Heights, NSW 2234, Australia*

(Received 18 May 2012; accepted 12 June 2012; published online 2 July 2012)

We report on the *in situ* polarized  $^3\text{He}$  neutron polarization analyzer developed for the *time-of-flight* Magnetism Reflectometer at the Spallation Neutron Source at Oak Ridge National Laboratory. Using the spin exchange optical pumping method, we achieved a  $^3\text{He}$  polarization of  $76\% \pm 1\%$  and maintained it for the entire three-day duration of the test experiment. Based on transmission measurements with unpolarized neutrons, we show that the average analyzing efficiency of the  $^3\text{He}$  system is 98% for the neutron wavelength band of 2–5 Å. Using a highly polarized incident neutron beam produced by a supermirror bender polarizer, we obtained a flipping ratio of  $>100$  with a transmission of 25% for polarized neutrons, averaged over the wavelength band of 2–5 Å. After the cell was depolarized for transmission measurements, it was reproducibly polarized and this performance was maintained for three weeks. A high quality polarization analysis experiment was performed on a reference sample of Fe/Cr multilayer with strong spin-flip off-specular scattering. Using a combination of the position sensitive detector, time-of-flight method, and the excellent parameters of the  $^3\text{He}$  cell, the polarization analysis of the two-dimensional maps of reflected, refracted, and off-specular scattered intensity *above* and *below* the horizon were obtained, simultaneously. [<http://dx.doi.org/10.1063/1.4731261>]

## **I. INTRODUCTION**

In recent years, polarized  $^3\text{He}$  neutron spin filters have been widely used as neutron polarizers and analyzers in various neutron scattering experiments at major neutron facilities around the world.<sup>1–4</sup> In order to be used as spin filters,  $^3\text{He}$  gas is contained in a glass cell and is polarized using either metastability exchange optical pumping (MEOP),<sup>5</sup> or spin exchange optical pumping (SEOP).<sup>6</sup> Although there have been considerable achievements in extending the lifetime of the polarization of the  $^3\text{He}$  gas,<sup>7</sup> the polarization of  $^3\text{He}$  unavoidably degrades and needs to be repolarized. The conventional application of polarized  $^3\text{He}$  as a spin filter involves an *ex situ* facility where the  $^3\text{He}$  cell is polarized outside the neutron beam. After the  $^3\text{He}$  cell is polarized using MEOP (Refs. 1 and 2) or SEOP (Refs. 3, 4, and 8), it is transported to the neutron beam for an experiment. The decay of cell polarization results in time dependence of the neutron polarization and transmission, which must be taken into account in the data analysis.<sup>9</sup> In addition, the overall performance of the experiment suffers from the time dependent degradation of the polarization and transmission of the neutron beam. To overcome the disadvantages of *ex situ* polarized  $^3\text{He}$  spin filters, *in situ* pumping using the SEOP method was developed.<sup>10–12</sup> For *in situ* pumping, the  $^3\text{He}$  cell with the polarizing system is installed on the beamline and is a part of the instrument.

When saturated, the  $^3\text{He}$  polarization stays constant throughout the entire experiment. However, until now apart from the first reports mentioned above, there have not been reports on a routine application of *in situ* SEOP systems in neutron scattering experiments due to several issues connected to the limited space on typical instruments and possibly due to high temperature and high power lasers. Here, we report on the successful development of the *in situ* polarized  $^3\text{He}$  neutron polarization analyzer developed for the *time-of-flight* Magnetism Reflectometer at the Spallation Neutron Source (SNS) at Oak Ridge National Laboratory (ORNL).

## **II. THE *IN SITU* PUMPING SYSTEM**

We have developed an *in situ* polarized  $^3\text{He}$  pumping system for use on neutron scattering beamlines at both reactor and spallation based neutron sources.<sup>13,14</sup> An earlier prototype of this *in situ* system was described in detail previously<sup>14,15</sup> where a proof-of-principle experiment using the polarization analysis of four neutron spin-states was reported.<sup>16</sup> Those first experiments showed that for a time-of-flight experiment with high polarization efficiency and transmission, it is necessary to improve considerably the polarization of  $^3\text{He}$  in order to use it for these kinds of experiments. Moreover, heat from the lasers and oven elevated the temperature at the beamline, which was unacceptable for the normal operation of the beamline electronics.

<sup>a)</sup>Electronic mail: tongx@ornl.gov.



FIG. 1. A typical cylindrical  $^3\text{He}$  cell. The cell is filled with  $^3\text{He}$  and  $\text{N}_2$  gas, as well as alkali metal, usually rubidium (Rb) and potassium (K). The cell described above is not the same but analogous to the cell we used in the present study.

We have made several significant design changes to the prototype system in order to improve the neutron transmission as well as the efficiency of the polarization analysis. These include the careful fabrication of a new cell, implementation of a better configuration for the heating and cooling systems as well as development of an optimized laser optics configuration for the optical pumping with improved laser collimation, and a narrower laser wavelength band. Optimization of the gas thickness of the  $^3\text{He}$  spin filter for a time-of-flight instrument using a wavelength band is more difficult than for a monochromatic beam because it is necessary to balance between acceptably high polarization for the short wavelength neutrons and an acceptable high transmission for long wavelength neutrons.

The cylindrically shaped  $^3\text{He}$  cell labeled “Hokie” (Figure 1, a typical  $^3\text{He}$  cell, not the cell “Hokie”) has an outer diameter of 6 cm and an overall length of 8 cm. A detailed schematic drawing of the new system is shown in Figure 2. The cell was blown from boron-free, aluminosilicate glass in the glass shop at ORNL. After being cleaned, the cell was filled with a mixture of 2.3 bar of  $^3\text{He}$  gas, 0.12 bars of  $\text{N}_2$  gas, and traces of rubidium (Rb) and potassium (K). In the previous setup, we were using electrical heating<sup>15</sup> to

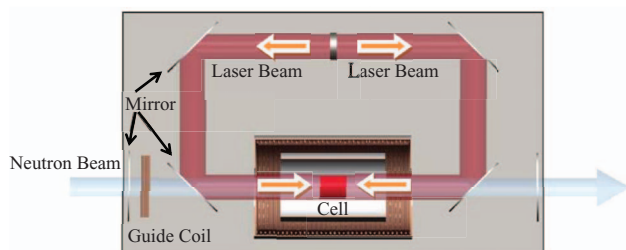


FIG. 2. The scheme of the *in situ*  $^3\text{He}$  pumping system.

vaporize the alkali. Even though the use of electrical heating does not interfere significantly with the optical pumping process or affect the final polarization of the  $^3\text{He}$  cell by a noticeable percentage, the electrically conducting heating pads do affect the nuclear magnetic resonance (NMR) measurements employed to monitor the relative  $^3\text{He}$  polarization. For this reason, we switched to using a forced hot air heating method, which had worked very well in the past but is more cumbersome than the electric heating method. When using forced hot air, compressed air is heated by a 1200 W air heater and flowed through the oven to maintain a cell temperature of 200 °C. In order to prevent the overheating of the components other than the oven, copper tubing is coiled between the solenoid and the  $\mu$ -metal shielding (see Figure 2) through which cooling water is continuously flowed.

The whole assembly, including the pumping system with the  $^3\text{He}$  cell is housed in a rectangular enclosure shielded by laser panels, which are interlocked with the laser in order to fulfill the safety requirements and be certified for routine use in experiments on the Magnetism Reflectometer. The entire enclosed  $^3\text{He}$  assembly is mounted on a table with a motorized lift and can be automatically positioned in the neutron beam. The front and back panels have 0.5 mm thick Si windows with dielectric coatings (to preserve laser light circular polarization) for the neutron beam to enter and exit.<sup>14</sup>

During the operation, the system is controlled by a computer and is completely automated. We use NMR methods to monitor and control the polarization. Free induction decay (FID), which provides a signal linearly proportional to the polarization, was used to monitor the  $^3\text{He}$  polarization. The signal was constant to within 0.25% during the three-day experiment period. After the test, we started the commissioning of the system. For the following three weeks, the FID stayed the same, which indicates a constant  $^3\text{He}$  polarization. In addition, we use adiabatic fast passage (AFP) to reverse the  $^3\text{He}$  polarization.<sup>13</sup> In order to perform polarization analysis for both neutron spin states, we use AFP to flip the  $^3\text{He}$  spin, which takes about 1 s. After spin flip, the circularly polarized laser light is no longer in the “correct” state to polarize  $^3\text{He}$ . Using an electronically controlled liquid crystal retarder, we are able to change the retardance from  $\frac{1}{4}$  wave to  $\frac{3}{4}$  wave instantaneously, thus switching left circularly polarized light to right circularly polarized light, and vice versa. We have used laser light of both helicities to optically pump  $^3\text{He}$  and in both cases, the saturated  $^3\text{He}$  polarizations are the same. The entire procedure of reversing  $^3\text{He}$  polarization usually takes less than 10 s to perform.

It is foreseen that the AFP will be incorporated in the Data Acquisition System (DAS) and will be performed automatically during the experiment. The performance of the whole  $^3\text{He}$  system will allow the instrument staff to operate it for the users’ experiments.

### III. $^3\text{He}$ CELL TRANSMISSION MEASUREMENT: UNPOLARIZED NEUTRON BEAM

We measured the neutron transmission through the cell to determine the analyzing power of the spin filter and the

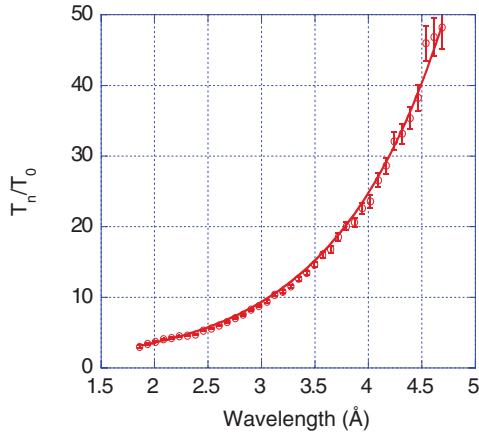


FIG. 3. Results for  $\frac{T_n}{T_0}(\lambda)$  vs. neutron wavelength along with a fit (solid line) to  $\frac{T_n}{T_0}(\lambda) = \cosh(n\sigma_0 l \lambda P_{\text{He}})$ . The fit yields  $n\sigma_0 l P_{\text{He}} = 0.965 \pm 0.003 \text{ \AA}^{-1}$ . The error bars shown in all figures are determined by statistical error.

$^3\text{He}$  polarization. The transmissions of unpolarized neutrons through unpolarized ( $T_0$ ) and polarized  $^3\text{He}$  ( $T_n$ ) are given by the following equations:

$$T_0(\lambda) = T_e \exp(-n\sigma_0 l \lambda), \quad (1)$$

$$T_n(\lambda) = T_e \exp(-n\sigma_0 l \lambda) \cosh(n\sigma_0 l \lambda P_{\text{He}}), \quad (2)$$

where  $T_e$  is normally defined as the transmission through the empty glass cell. However, for our measurements, it was impractical to remove the cell. Hence, in our case,  $T_e$  refers to the transmission of the entire assembly that includes the cell, 4 silicon mirrors, and 2 sapphire windows (for the oven).  $n$  is the  $^3\text{He}$  number density;  $\sigma_0$  is the  $^3\text{He}$  absorption cross section for neutrons per  $\text{\AA}$ ;  $l$  is the length of the cell;  $\lambda$  is the neutron wavelength, and  $P_{\text{He}}$  is the  $^3\text{He}$  polarization. We will refer to the product  $n\sigma_0 l$  as the  $^3\text{He}$  cell thickness.

Dividing Eq. (2) by Eq. (1) to eliminate the contribution of the empty transmission, the following equation is obtained

$$\frac{T_n}{T_0}(\lambda) = \cosh(n\sigma_0 l \lambda P_{\text{He}}). \quad (3)$$

During the experiment, we first measured the neutron transmission through the polarized  $^3\text{He}$  cell  $T_n(\lambda)$ , then we depolarized the cell and measured the unpolarized transmission  $T_0(\lambda)$ . From the fit of Eq. (3) to the experiment data, we obtained the following result:

$$n\sigma_0 l P_{\text{He}} = 0.965 \pm 0.003 \text{ \AA}^{-1}. \quad (4)$$

The data and fit are presented in Figure 3. A small dependence on the wavelength band for the fit was observed; hence, the uncertainty was enlarged to accommodate this variation.

In order to obtain the  $^3\text{He}$  polarization  $P_{\text{He}}$ , we need to determine the cell thickness. Whereas, in principle, we could fit these data to determine  $T_e$  and the cell thickness, we found that the results were not consistent for different neutron wavelength bands. Hence, we determined the transmission  $T_e(\lambda)$  experimentally by measuring the neutron intensity with and without the mirrors, windows, and an empty unfilled cell. For this measurement, we used a similar prototype unfilled cell, and we estimate that the glass thickness for the two cells was similar. The measured average transmission was  $T_e = 0.82$ .

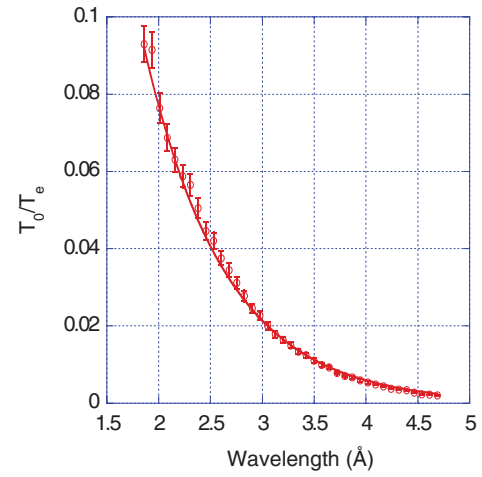


FIG. 4.  $\frac{T_0}{T_e}$  as a function of neutron wavelength along with a fit (solid line) to  $\frac{T_0(\lambda)}{T_e(\lambda)} = \exp(-n\sigma_0 l \lambda)$ . Based on fitting over different wavelength bands a cell thickness of  $1.270 \pm 0.013 \text{ \AA}^{-1}$  is obtained. Combining with the fit result from Figure 3, we obtain the  $^3\text{He}$  polarization to be  $76\% \pm 1\%$ .

We then fit  $\frac{T_0}{T_e}$  using Eq. (1). A cell thickness

$$n\sigma_0 l = 1.270 \pm 0.013 \text{ \AA}^{-1} \quad (5)$$

was obtained (see Figure 4). We assigned the uncertainty by fitting over different neutron wavelength bands.

Using the experimentally obtained value for the  $^3\text{He}$  cell thickness, the  $^3\text{He}$  polarization was determined to be  $76\% \pm 1\%$  as follows from Eqs. (4) and (5). The uncertainty is dominated by the uncertainty in the cell thickness, which includes the uncertainty of the fit and a contribution from using a different cell for the  $T_e$  measurement.

#### IV. POLARIZED NEUTRON TRANSMISSION MEASUREMENT: POLARIZATION ANALYSIS

In the standard Magnetism Reflectometer configuration, a supermirror bender was used to polarize the beam and an adiabatic RF-gradient spin flipper<sup>17</sup> was employed for neutron spin reversal. In order to provide the adiabatic rotation from vertical to horizontal along the beam direction of the polarized neutrons from the sample position to the  $^3\text{He}$  cell, we installed an additional guide field with a double coil system. The first coil has an adjustable vertical field towards the sample position; the second split coil consists of two parts. The first part provides a horizontal field with an increasing gradient up to the  $^3\text{He}$  analyzer housing and the second part is installed inside of the  $^3\text{He}$  housing. We measured the spectra of the intensity of the polarized neutron beam with neutrons spin-up (parallel to the direction of the guide field)  $T_+(\lambda)$  and spin-down (opposite to the direction of the guide field)  $T_-(\lambda)$ . The wavelength dependence of the flipping ratio ( $F$ ) is defined as

$$F(\lambda) = \frac{T_+(\lambda)}{T_-(\lambda)}. \quad (6)$$

Figure 5 shows the measured flipping ratio as a function of neutron wavelength. The flipping ratio was used to



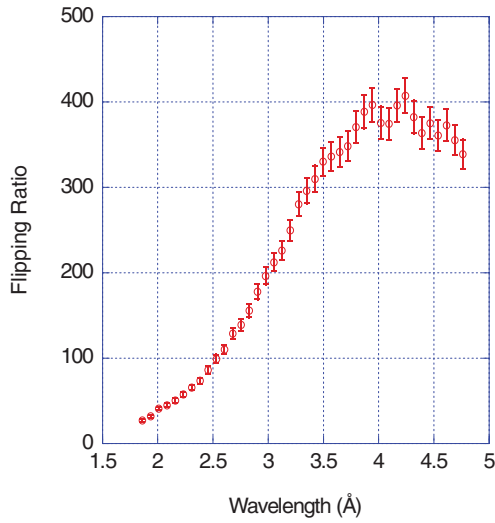


FIG. 5. The measured flipping ratio  $F$  vs. neutron wavelength. This is a combined flipping ratio, which takes into account the efficiency of the supermirror polarizer, the spin-flipper, the  $^3\text{He}$  analyzer, and spin transport efficiency (guide fields) as described in the text.

determine the polarization of the neutron beam incident on the  $^3\text{He}$  analyzer,  $P_1(\lambda)$ , which is determined by the polarizing efficiency of the supermirror and the spin transport efficiency. For the polarized neutron beam with polarization  $P_1(\lambda)$  passing through the  $^3\text{He}$  cell with polarizing efficiency  $P_2(\lambda)$ , the following equation can be used:

$$P_1(\lambda) P_2(\lambda) = \frac{F - 1}{F + 1}, \quad (7)$$

where we have assumed that both the spin flip efficiency and the spin transport efficiency are close to 100%, which was confirmed in our earlier paper.<sup>15</sup> The flipping ratio increases from 30 to 375 within the wavelength band of 2–5 Å. In order to test the limiting conditions, the experiment was performed with the cross-sections of the beam *larger* than a typical cross-section of the beam for the reflectometry configuration on the Magnetism Reflectometer. The height of the beam in the sample position of 10 mm and 15 mm and the width of 0.5–1 mm was tested. The flipping ratio did not degrade with increasing the cross sections. In Figure 6, we show  $P_1(\lambda)$  extracted from Eq. (7) using  $P_2(\lambda)$  determined from the unpolarized measurements discussed in Sec. III.

## V. POLARIZATION ANALYSIS OF REFLECTED AND MAGNETIC OFF-SPECULAR SCATTERING

Polarized neutron scattering techniques are very important and powerful tools to study the structures of magnetic materials and soft matters. Polarized neutron reflectometry (PNR) plays an important role for the exploration of magneto- and spintronic structures.<sup>18,19</sup> Well-known systems extensively studied include exchange bias systems between ferromagnetic and antiferromagnetic films, exchange coupled magnetic superlattices, exchange spring valves between soft and hard magnetic films. In addition to the studies of uniform layered systems, neutron scattering is applied to the exploration of periodic magnetic arrays, such as nanodots, stripes,

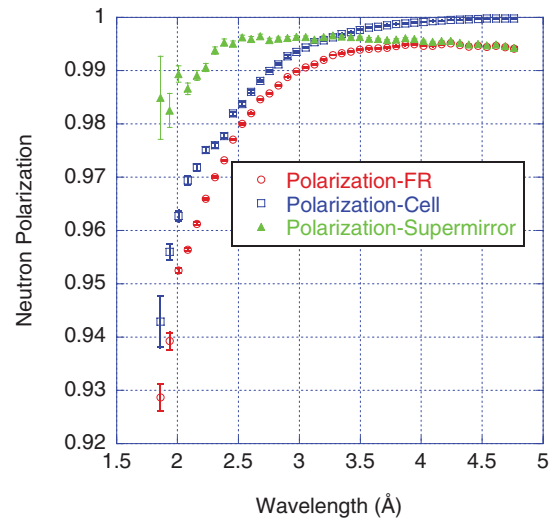


FIG. 6. Experimental neutron polarization plots as functions of neutron wavelength. The blue curve (“polarization-cell”) is obtained from the unpolarized neutron transmission measurement and corresponds to the analyzing efficiency  $P_2(\lambda)$  of the  $^3\text{He}$  analyzer. The red curve (“polarization-FR”) shows the polarizer and  $^3\text{He}$  analyzer polarizing efficiency product  $P_1(\lambda) P_2(\lambda) = \frac{F-1}{F+1}$ , as described in the text. The green curve (“polarization-supermirror”) shows the polarizing efficiency of the supermirror polarizer  $P_1(\lambda)$  determined from the ratio of the red and blue curves.

and islands on the submicrometer scale.<sup>20</sup> The scattering signal consists of a specularly reflected line and an off-specular scattered two-dimensional pattern.<sup>21</sup> For magnetic systems, this intensity contains information about the transverse and lateral structures of the sample, including the chemical composition and magnetic structure. In order to extract the full information about the magnetization vector distribution, polarization analyzers of the scattered intensity are necessary. They should have a broad cross section, high level of polarization, and good transmission.<sup>22,23</sup> Full polarization analysis of the two-dimensional intensity maps permits the reconstruction of the transverse and lateral profiles of the magnetization vector distribution. However, the capability of providing a constant polarization analysis of the broad band beam of the scattered intensity with a high analyzing efficiency and transmission is still limited worldwide. Here, we used the above described  $^3\text{He}$  cell as an analyzer in the experiment.

For the test experiment, we used a sample analogous to the one used in an earlier paper.<sup>21</sup> A multilayer sample of (001)  $^{57}\text{Fe}(6.7 \text{ nm})/\text{Cr}(-1.2 \text{ nm})$  with 12 bilayers was grown with molecular beam epitaxy on (110)  $\text{Al}_2\text{O}_3$  substrates covered with a 6.8 nm of Cr buffer layer. This sample shows an anti-ferromagnetic inter-layer exchange coupling and an in-plane magnetic domain structure. The PNR experiment was performed in an external magnetic field of 30 mT applied in-plane of the sample after saturation in a field of 1 T.

Using the two-dimensional position sensitive detector and the neutron beam with a wavelength band from 2–5 Å, we measured in alternation the “+ +” and “– +” spin cross sections, using an adiabatic spin-flipper in front of the sample. After this measurement was complete, we changed the direction of the  $^3\text{He}$  polarization by AFP and repeated the experiment to obtain the “+ –” and “– –” spin cross sections. The schematic of the experiment is shown in

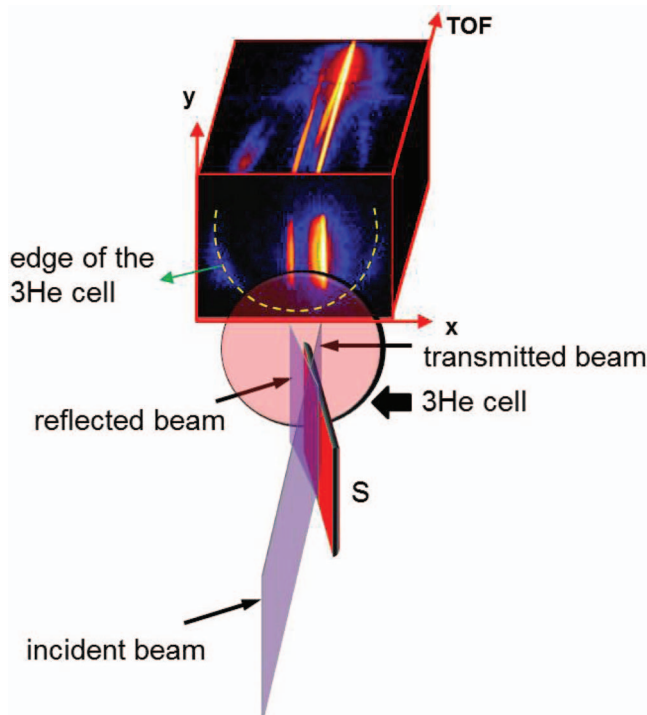


FIG. 7. The schematic view of the reflectometry experiment, showing sample (S), incident, reflected, and transmitted polarized neutron beams. Incoming neutron beam is polarized by supermirror bender polarizer followed by an adiabatic RF-gradient neutron spin flipper (not shown in the figure). The  $^3\text{He}$  cell covers the cross sections of both the reflected and transmitted beams. The intensity is recorded by a position sensitive detector and presented in three-dimensional coordinates. The dashed line indicates the area being analyzed by the cell.

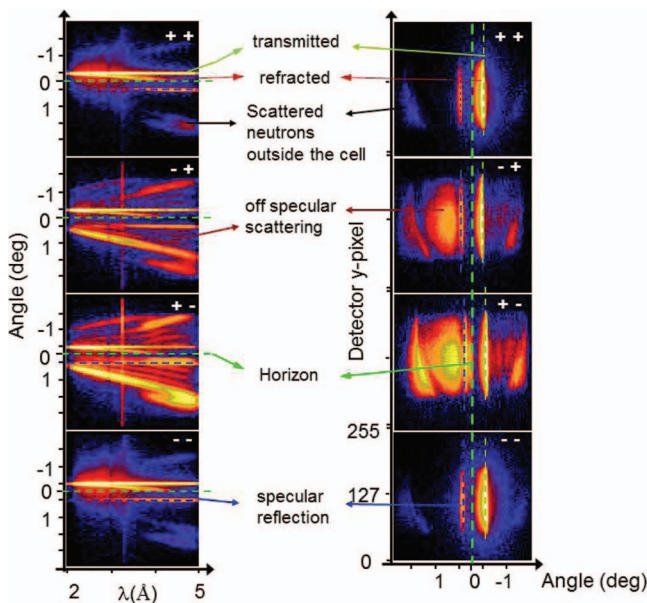


FIG. 8. Experimental data from the Fe/Cr multilayer measured in the external magnetic field of 30 mT. The left panel shows the wavelength dependence of the specularly reflected, off-specularly scattered, and transmitted intensities for the four spin-states. The right panel represents the same data, shown in the coordinates of the position sensitive detector (PSD) and being integrated over the TOF.

Figure 7. The polarized neutron beam impinges on the surface of the sample at a grazing incident angle. The reflected, scattered, and transmitted beams pass through the polarized  $^3\text{He}$  cell so that the polarization of the intensity coming from the sample is analyzed and recorded by a position sensitive detector (coordinates X and Y) and the time-of-flight electronics (coordinate TOF). The experimental intensity corresponding to the four neutron spin-states is presented in Figure 8. The intensity was measured *simultaneously above and below* the horizon with polarization analysis. The data show the reflected, off-specular scattered, and transmitted intensity analyzed with excellent quality. The left panel represents the wavelength dependence of the specularly reflected, off-specularly scattered, and transmitted intensity for the four spin-states. The detailed description of the scattered intensity goes beyond the scope of the present paper. However, we would like to point out that the *asymmetry* in the spin-flip off-specular scattering is clearly demonstrated in the present experiment. The details of the magnetic off-specular scattering, the origin of its asymmetry, and the theoretical model within the distorted wave Born approximation were explained in details in the earlier papers.<sup>24,25</sup>

## VI. CONCLUSIONS

In conclusion, we successfully constructed an *in situ* polarized  $^3\text{He}$  neutron polarization analyzer for the *time-of-flight* Magnetism Reflectometer at the SNS. Using the SEOP method, we achieved a  $^3\text{He}$  polarization of  $76\% \pm 1\%$  and maintained it over a three-week period. The average analyzing efficiency of the  $^3\text{He}$  system is 98% for the neutron wavelength band of 2–5 Å and a flipping ratio of  $>100$  for 2.5 Å neutrons was achieved. The transmission of 25% averaged over a wavelength band of 2–5 Å of the polarized neutron beam was obtained. A high quality polarization analysis experiment was performed on a reference sample of Fe/Cr multilayer with a strong spin-flip off-specular scattering. Using a combination of the position sensitive detector, time-of-flight method, and the polarized  $^3\text{He}$  cell, the polarization analysis of the two-dimensional map of reflected, refracted, and off-specular scattered intensity *above and below* the horizon were obtained, simultaneously. Further exploitation of neutron polarization analyzers based on polarized  $^3\text{He}$  is in progress for a routine maintenance during experiments.

## ACKNOWLEDGMENTS

Research at Oak Ridge National Laboratory's Spallation Neutron Source was sponsored by the Scientific User Facilities Division, Office of Basic Energy Sciences, U.S. Department of Energy. The contributions of T. R. Gentile to the analysis and documentation of this work were supported in part by the Office of Basic Energy Sciences, U.S. Department of Energy.

<sup>1</sup>E. Lelievre-Berna, *Physica B* **397**(1-2), 162–167 (2007).

<sup>2</sup>E. Lelievre-Berna and A. Ioffe, *Neutron News* **20**(1), 33 (2009).

<sup>3</sup>D. M. Pajerowski, V. O. Garlea, E. S. Knowles, M. J. Andrus, M. F. Dumont, S. E. Nagler, X. Tong, D. R. Talham, and M. W. Weisel, "Magnetic Neutron Scattering of Thermally Quenched K-Co-Fe Prussian Blue Analogue Photomagnet," *Phys. Rev. B* (submitted).

- <sup>4</sup>W. C. Chen, R. Erwin, J. W. McIver, S. Watson, C. B. Fu, T. R. Gentile, J. A. Borchers, J. W. Lynn, and G. L. Jones, *Physica B* **404**(17), 2663–2666 (2009).
- <sup>5</sup>K. H. Andersen, R. Chung, V. Guillard, H. Humblot, D. Jullien, E. Lelievre-Berna, A. Petoukhov, and F. Tasset, *Physica B* **356**(1-4), 103–108 (2005).
- <sup>6</sup>T. G. Walker and W. Happer, *Rev. Mod. Phys.* **69**(2), 629–642 (1997).
- <sup>7</sup>W. C. Chen, T. R. Gentile, C. B. Fu, S. Watson, G. L. Jones, J. W. McIver, and D. R. Rich, *J. Phys.: Conf. Ser.* **294**, 012003 (2011).
- <sup>8</sup>T. R. Gentile, E. Babcock, J. A. Borchers, W. C. Chen, D. Hussey, G. L. Jones, W. T. Lee, C. F. Majkrzak, K. V. O'Donovan, W. M. Snow, X. Tong, S. G. E. T. Velthuis, T. G. Walker, and H. Yan, *Physica B* **356**(1-4), 96–102 (2005).
- <sup>9</sup>K. Krycka, W. Chen, J. Borchers, B. Maranville, and S. Watson, *J. Appl. Crystallogr.* **45**, 546–553 (2012).
- <sup>10</sup>G. L. Jones, J. Baker, W. C. Chen, B. Collett, J. A. Cowan, M. F. Dias, T. R. Gentile, C. Hoffmann, T. Koetzle, W. T. Lee, K. Littrell, M. Miller, A. Schultz, W. M. Snow, X. Tong, H. Yan, and A. Yue, *Physica B* **356**(1-4), 86–90 (2005).
- <sup>11</sup>E. Babcock, S. Boag, K. H. Andersen, M. Becker, C. Beecham, F. Bordenave, J. Chastagnier, W. C. Chen, R. Chung, T. E. Chupp, S. Elmore, P. Fouilloux, T. R. Gentile, D. Jullien, E. Lelievre-Berna, P. Mouveau, A. Petoukhov, M. Revert, and T. Soldner, *Physica B* **404**(17), 2655–2658 (2009).
- <sup>12</sup>T. E. Chupp, K. P. Coulter, M. Kandes, M. Sharma, T. B. Smith, G. Jones, W. C. Chen, T. R. Gentile, D. R. Rich, B. Lauss, M. T. Gericke, R. C. Gillis, S. A. Page, J. D. Bowman, S. I. Penttila, W. S. Wilburn, M. Dabaghyan, F. W. Hersman, and M. Mason, *Nucl. Instrum. Methods Phys. Res. A* **574**(3), 500–509 (2007).
- <sup>13</sup>G. L. Jones, F. Dias, B. Collett, W. C. Chen, T. R. Gentile, P. M. B. Piccoli, M. E. Miller, A. J. Schultz, H. Yan, X. Tong, W. M. Snow, W. T. Lee, C. Hoffmann, and J. Thomison, *Physica B* **385–386**, 1131–1133 (2006).
- <sup>14</sup>W. T. Lee, X. Tong, J. Pierce, M. Fleenor, A. Ismaili, J. L. Robertson, W. C. Chen, T. R. Gentile, A. Hailemariam, R. Goyette, A. Parizzi, V. Lauter, F. Klose, H. Kaiser, C. Lavelle, D. V. Baxter, G. L. Jones, J. Wexler, and L. McCollum, in *Proceedings of the International Conference on Neutron Scattering 2009*, *J. Phys.: Conf. Ser.* **251**, 012086 (2010).
- <sup>15</sup>X. Tong, J. Pierce, W. T. Lee, M. Fleenor, W. C. Chen, G. L. Jones, and J. L. Robertson, in *Proceedings of the International Conference on Neutron Scattering 2009*, *J. Phys.: Conf. Ser.* **251**, 012087 (2010).
- <sup>16</sup>V. Lauter, H. Ambaye, R. Goyette, W. T. H. Lee, and A. Parizzi, *Physica B* **404**(17), 2543–2546 (2009).
- <sup>17</sup>A. N. Bazhenov, V. M. Lobashev, A. N. Pirozhkov, and V. N. Slusar, *Nucl. Instrum. Methods Phys. Res. A* **332**(3), 534–536 (1993).
- <sup>18</sup>K. Theis-Brohl, B. P. Toperverg, A. Westphalen, H. Zabel, J. McCord, V. Hoink, J. Schmalhorst, G. Reiss, T. Weis, D. Engel, A. Ehresmann, and U. Rucker, *Superlattices Microstruct.* **41**(2-3), 104–108 (2007).
- <sup>19</sup>M. Gibert, P. Zubko, R. Scherwitzl, J. Iniguez, and J. M. Triscone, *Nature Mater.* **11**(3), 195–198 (2012).
- <sup>20</sup>R. Pynn, “Neutron Scattering,” in *McGraw-Hill Yearbook of Science and Technology* (McGraw-Hill Professional, 2009), p. 252.
- <sup>21</sup>V. Lauter-Pasyuk, H. J. Lauter, B. P. Toperverg, L. Romashev, and U. Ustinov, *Phys. Rev. Lett.* **89**(16), 167203 (2002).
- <sup>22</sup>W. C. Chen, T. R. Gentile, K. V. O'Donovan, J. A. Borchers, and C. F. Majkrzak, *Rev. Sci. Instrum.* **75**(10), 3256–3263 (2004).
- <sup>23</sup>D. Hussey, S. Fan, B. Neff, C. Bailey, W. M. Snow, D. Rich, A. K. Thompson, T. R. Gentile, S. G. E. T. Velthuis, and G. P. Felcher, *Appl. Phys. A: Mater. Sci. Process.* **74**, S234–S236 (2002).
- <sup>24</sup>V. Lauter-Pasyuk, H. J. Lauter, B. Toperverg, O. Nikonov, E. Kravtsov, L. Romashev, and V. Ustinov, *J. Magn. Magn. Mater.* **226**, 1694–1696 (2001).
- <sup>25</sup>B. Toperverg, O. Nikonov, V. Lauter-Pasyuk, and H. J. Lauter, *Physica B* **297**(1-4), 169–174 (2001).